A Medium Bandgap Dimeric Acceptor with High Open-Circuit Voltage for Efficient Organic Solar Cells

Baofa Lan[a], Shaohui Yuan[a], Yanyi Zhong[b], Wenkai Zhao[a], Jia Wang[a], Wendi Shi[c], Guankui Long[a]*, Oleg A. Rakitin[d], Jiangbin Zhang[b][e][f], Kai Han[b][e]*, Bin Kan[a]*, Yongsheng Chen[c]

[a] School of Materials Science and Engineering, National Institute for Advanced Materials, Nankai University, Tianjin 300350, China.

[b] College of Advanced Interdisciplinary Studies, National University of Defense Technology, Changsha 410073, China.

[c] State Key Laboratory and Institute of Elemento-Organic Chemistry, Frontiers Science Center for New Organic Matter, The Centre of Nanoscale Science and Technology and Key Laboratory of Functional Polymer Materials, Renewable Energy Conversion and Storage Center (RECAST), College of Chemistry, Nankai University, Tianjin 300071, China.

[d] N. D. Zelinsky Institute of Organic Chemistry Russian Academy of Sciences, 47 Leninsky Prospekt, Moscow, Russia.

[e] Nanhu Laser Laboratory, National University of Defense Technology, Changsha 410073, China

[f] Hunan Provincial Key Laboratory of High Energy Laser Technology, National University of Defense Technology, Changsha 410073, China.

Corresponding E-mails: kanbin04@nankai.edu.cn (B.K.); hankai0071@nudt.edu.cn (K. H.); longgk09@nankai.edu.cn (G. L.)

Contents

1. Materials and Synthesis

Polymer donor PM6 (Mn = 51 kDa, Mw = 124 kDa, PDI = 2.43), 2-(5-bromo-3-oxo-2,3-dihydro-1H-inden-1-ylidene)malononitrile (INCN-Br), 5,7-bis(trimethylstannyl)-2,3-dihydrothieno[3,4-b][1,4]dioxine and the ending unit 2-(5,6-difluoro-3-oxo-2,3-dihydro-1H-inden-1-ylidene)malononitrile (INCN-2F) were purchased from Solarmer Material (Beijing) Inc, Woerjiming (Beijing) Technology Development Institute, Macklin and Derthon, respectively. Starting material 1 was synthesized according to the general method reported before.[1] Unless otherwise specified, all the other reagents and chemicals were used directly without further purification, which purchased from commercial suppliers.

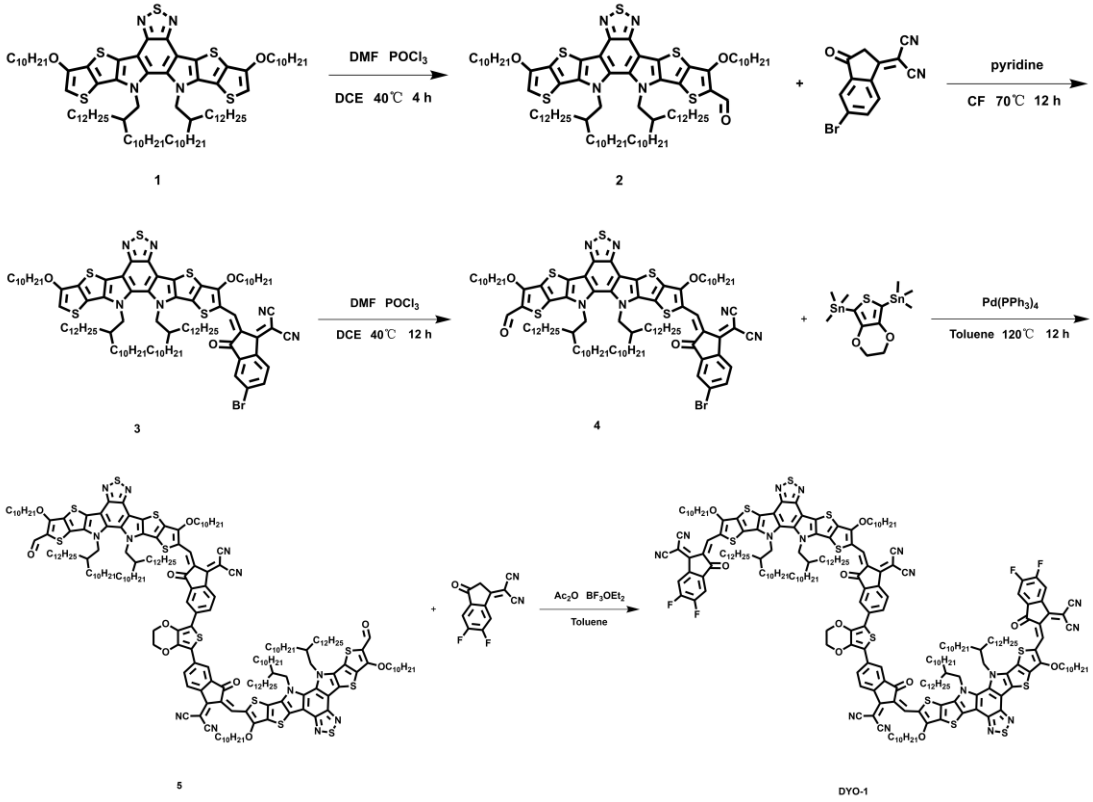

Scheme S1. The synthetic route of DYO-1.

Synthesis of Compound 2: Compound 1 (2.00 g, 1.40 mmol, 1.0 eq) was dissolved in 250 mL two-necked round bottom flask with 50 mL DCE. Then the system has been protected by argon. DMF (0.31 g, 4.21 mmol, 3 eq) and $POCl_3$ (0.65 g, 4.21 mmol, 3eq) were injected into the mixture. The mixture was heated to 40℃ for 4 h. The mixture

was quenched with saturated aqueous solution of sodium acetate and then extracted with dichloromethane. The organic layers were combined and dried over anhydrous Na_2SO_4. After removal of the solvent, the crude product was purified by silica gel column chromatography (petroleum ethe:dichloromethane = 4:1, v/v) to obtain compound 2 (1.22 g, 60%).

Data for compound 2: ^{1}H NMR (400MHz, $CDCl_3$, ppm) δ 10.10 (s, 1H), 6.33 (s, 1H), 4.69 (t, *J* = 4.0 Hz, 2H), 4.59 (t, *J* = 8.0 Hz, 4H), 4.15 (t, *J* = 8.0 Hz, 2H), 2.11-1.86 (m, 7H), 1.60-1.49 (m, 5H), 1.44-1.13 (m, 66H), 1.07-0.95 (m, 14H), 0.90-0.72 (m, 40H). ^{13}C NMR (101MHz, $CDCl_3$, ppm) δ 180.91, 158.78, 151.27, 147.67, 147.33, 137.79, 135.96, 134.32, 133.49, 130.69, 130.42, 128.50, 123.10, 121.97, 121.20, 113.17, 110.75, 96.40, 73.13, 70.81, 32.02, 31.98, 31.94, 30.35, 30.29, 29.98, 29.74, 29.70, 29.66, 29.61, 29.58, 29.49, 29.45, 29.38, 29.35, 29.27, 26.11, 25.87, 25.50, 25.41, 22.77, 22.75, 14.19,14.16. MS (m/z, MALDI): Calc. for $[C_{87}H_{142}N_4O_3S_5]H^+$ 1451.97, found: 1450.96.

Synthesis of Compound 3: Compound 2 (1.00 g, 0.69 mmol, 1 eq) and INCN-Br (0.38 mg, 1.38 mmol, 2eq) were dissolved in 250 mL two-necked round bottom flask with 30 mL CF. Then the system was protected by argon. Pyridine (1.0 mL) was injected into the mixture. Then the mixture was heated to 70℃ for 12 h under the protection of argon. The reaction mixture was precipitated in 30 mL methanol. Finally, the precipitate was purified by column chromatography on silica gel with the eluent of petroleum ether:dichloromethane (v:v = 3:1) obtained Compound 3 (0.97 g, 82%).

Data for compound 3: ^{1}H NMR (400MHz, $CDCl_3$, ppm) δ 9.23 (s, 1H), 8.38 (d, *J* = 8.0 Hz, 1H), 7.87 (d, *J* = 2.0 Hz, 1H), 7.64 (dd, *J* = 4.0, 4.0 Hz, 1H), 6.38 (s, 1H), 4.75-4.62 (m, 6H), 4.16 (t, *J* = 8.0 Hz, 2H), 2.21-2.06 (m, 2H), 2.01-1.86 (m, 4H), 1.58-1.50 (m, 4H), 1.39-1.36 (m, 24H), 1.26-1.10 (m, 44H), 1.04-0.96 (m,28H), 0.91-0.79 (m, 26H). ^{13}C NMR (101MHz, $CDCl_3$, ppm) δ 187.21, 162.55, 159.53, 151.31, 147.80, 147.30, 138.68, 138.60, 138.27, 138.21, 136.64, 136.49, 136.34, 134.23, 132.89, 130.13, 128.34, 126.89, 126.08, 125.87, 123.35, 121.92, 119.81, 116.71, 115.24, 114.40, 110.93, 74.07, 70.92, 66.15, 39.13, 38.82, 32.01, 31.97, 30.71, 30.44, 29.81, 29.76, 29.72, 29.65, 29.61, 29.53, 29.49, 29.46, 29.41, 29.36, 29.28, 26.11, 25.88, 25.76, 25.55,

22.76, 14.17. MS (m/z, MALDI): Calc. for $[C_{99}H_{145}BrN_6O_3S_5]H^+$ 1707.92, found: 1707.10.

Synthesis of Compound 4: Compound 3 (0.90 g, 0.53 mmol, 1.0 eq) was dissolved in 250 mL two-necked round bottom flask with 30 mL DCE. Then the system has been protected by argon. DMF (0.23 g, 3.16 mmol, 6 eq) and $POCl_3$ (0.48 g, 3.16 mmol, 6 eq) were injected into the mixture. The mixture was heated to 40℃ for 12 h. The mixture was quenched with saturated aqueous solution of sodium acetate and then extracted with dichloromethane. The organic layers were combined and dried over anhydrous Na_2SO_4. After removal of the solvent, the crude product was purified by silica gel column chromatography (petroleum ether:dichloromethane = 2:1, v/v) to obtain compound 4 (0.88 g, 96%).

Data for compound 4: ^{1}H NMR (400MHz, $CDCl_3$, ppm) δ 10.11 (s, 1H), 9.13 (d, *J* = 8.0 Hz 1H), 8.27 (d, *J* = 8.0 Hz, 1H), 7.81 (s, 1H), 7.56 (d, *J* = 8.0 Hz, 1H), 4.79-4.61 (m, 8H), 2.21-2.09 (m, 2H), 1.97-1.87 (m, 4H), 1.57-1.46 (m, 4H), 1.37-1.23 (m, 28H), 1.21-1.08 (m, 42H), 1.02-0.96 (m, 30H), 0.88-0.76 (m, 22H). ^{13}C NMR (101MHz, $CDCl_3$, ppm) δ 187.06, 180.97, 162.13, 159.07, 158.37, 147.44, 147.29, 138.57, 138.06, 137.70, 137.36, 137.06, 134.95, 132.60, 131.82, 129.99, 129.92, 128.48, 127.93, 127.45, 126.13, 122.37, 119.83, 115.52, 114.98, 113.18, 112.12, 74.02, 73.30, 66.89, 55.65, 39.24, 39.05, 31.99, 31.94, 30.73, 30.44, 29.99, 29.86, 29.75, 29.73, 29.68, 29.65, 29.59, 29.55, 29.43, 29.40, 29.37, 25.87, 25.52, 22.73, 14.14. MS (m/z, MALDI): Calc. for $[C_{100}H_{145}BrN_6O_3S_5]H^+$ 1735.91, found: 1735.24.

Synthesis of Compound 5: Compound 4 (0.88 g, 0.46 mmol, 1.0 eq), 5,7-bis(trimethylstannyl)-2,3-dihydrothieno[3,4-b][1,4]dioxine (97.03 mg, 0.21 mmol, 0.45 eq) and $Pd(PPh_3)_4$ (106.54 mg, 92.19 μmol, 0.2 eq) were dissolved in 100 mL two-necked round bottom flask with 35 mL toluene. Then the mixture was heated to reflux for 12 h under the protection of argon. After cooling to room temperature, the reaction mixture was extracted with dichloromethane. The organic layers were combined and dried over anhydrous Na_2SO_4. Finally, the precipitate was purified by column chromatography on silica gel with the eluent of petroleum ether:dichloromethane (v:v

= 1:1) obtained compound 5 (0.37 g, 47%).

Data for compound 5: ^{1}H NMR (400MHz, $CDCl_3$, ppm) δ 10.13 (s, 2H), 9.11 (s, 2H), 8.62 (d, *J* = 8.0 Hz, 2H), 8.07 (s, 2H), 7.82 (d, *J* = 8.0 Hz, 2H), 4.82-4.57 (m, 20H), 2.23-2.13 (m, 4H), 1.98-1.94 (m, 4H), 1.74 (s, 4H), 1.60-1.56 (m, 4H), 1.45-1.41 (m, 6H), 1.38-1.30 (m, 24H), 1.27-0.95 (m, 170H), 0.91-0.80 (m, 48H). ^{13}C NMR (101MHz, $CDCl_3$, ppm) δ 188.39, 181.07, 161.67, 159.27, 158.50, 147.54, 147.47, 141.33, 138.10, 137.77, 134.51, 132.90, 131.21, 130.19, 130.05, 129.85, 127.94, 127.68, 122.27, 119.79, 118.60, 116.65, 116.08, 115.22, 112.87, 112.47, 77.29, 73.93, 73.31, 65.49, 55.89, 39.04, 32.00, 31.97, 31.94, 30.53, 29.99, 29.84, 29.80, 29.76, 29.72, 29.68, 29.62, 29.59, 29.45, 29.42, 29.36, 25.87, 25.80, 25.74, 25.59, 22.75, 22.72, 14.18, 14.14. MS (m/z, MALDI): Calc. for $[C_{206}H_{294}N_{12}O_{10}S_{11}]H^+$ 3449.99, found: 3451.20.

Synthesis of Compound DYO-1: Compound 5 (150 mg, 43.46 μmol, 1 eq), INCN-2F (40.01 mg, 0.17 mmol, 4 eq) and Ac_2O (0.15 mL), BF_3OEt_2 (0.15 mL) were mixed in 100 mL single-necked round bottom flask with 15 mL toluene. Then the mixture was reacted 25 min at room temperature under the protection of argon. The reaction mixture was precipitated in 30 mL methanol. Finally, the precipitate was purified by column chromatography on silica gel with the eluent of petroleum ether:dichloromethane (v:v = 1:1) obtained DYO-1 (105 mg, 63%).

Data for DYO-1: MS (m/z, MALDI): Calc. for $[C_{230}H_{298}F_4N_{16}O_{10}S_{11}]H^+$ 3875.67, found: 3875.70.

2. Device Fabrication and Characterization

OPV devices fabrication. The OSCs were fabricated using a conventional structure comprising ITO/ hole transport layer (HTL)/Active layer/PNDIT-F3N/Ag, which the PEDOT:PSS used for HTL for PM6:DYO-1 binary OSC, 3-BPIC-F used for HTL for PM6:L8-BO-X binary OSC and PM6:L8-BO-X:DYO-1 ternary OSC. Initially, ITO-coated glass was cleaned with deionized water, acetone, and isopropyl alcohol through ultrasonication for 10 min sequentially. Subsequently, the surface of the ITO-coated glass was treated in an ultraviolet-ozone chamber for 20 min. A thin layer of 3-BPIC-F was deposited on the ITO substrate at 3000 rpm for 20 s and then annealed in air at 100°C for 5 min. Following this, the substrates were transferred to a glovebox filled with nitrogen. The active layer solutions of PM6:DYO-1 (1:1.2), PM6:L8-BO-X (1:1.1), and PM6:L8-BO-X:DYO-1 (1:1:0.1) were prepared by dissolving in *o*-xylene (*o*-XY) at donor concentrations of 8, 9, and 9 mg/mL, respectively. For the PM6:DYO-1 device, 100 wt% (of total weight) 2-methoxynaphthalene (2-MN) was used as a solid additive. In the cases of PM6:L8-BO-X and PM6:L8-BO-X:DYO-1 devices, 0.35 vol% 1,8-diiodooctane (DIO) was employed as a solvent additive. All solutions were stirred at 100°C for 3 h and then spin-coated after cooling to 80°C. The active layer was spun onto the 3-BPIC-F layer at 3000 rpm for 20 s, followed by thermal annealing at 90°C for 5 min. After cooling, a methanol solution of PNDIT-F3N (1 mg/mL) was spin-coated on top of the active layer at 3300 rpm for 20 s. Finally, an Ag electrode with a thickness of 120 nm was evaporated under a vacuum of 1×10^{-4} Pa. The active area of the device was 4 mm², and a shadow mask with an area of 3.24 mm² was utilized during the *J-V* testing.

The glue dispenser/spin coater (Brand-REESEEN, PvS-mini7) used in the lab are from Jiangyin J. Wanjia Technology Co., Ltd.

OPV devices characterization. The current density-voltage (*J-V*) curves of OSCs were recorded on a Keithley 2400 source-measure unit in a glove box filled with nitrogen. Enli SS-F5-3A solar simulator with AM 1.5 G was used as the light source, and the light intensity was 100 mW cm^{-2} which was calibrated by a standard Si solar cell (made by

Enli Technology Co., Ltd., Taiwan, and calibrated report can be traced to NREL). A QE-R Solar Cell Spectral Response Measurement System was used to measure the external quantum efficiency (EQE) values of the devices. A Veeco Dektak 150 profilometer was used to measure the thickness of the active layers.

3. Measurements and Instruments

Molecular dynamic (MD) simulations. All molecular dynamics simulations were conducted utilizing the GROMACS (2023.3) software package,[2] employing the GROMOS force field. The restrained electrostatic potential (RESP) fitting technique was applied to derive partial charges for each molecule.

For the PM6:DYO-1 blend film, 56 PM6 molecules (with 5 repeat units) and 99 DYO-1 molecules were randomly placed in a 50 × 50 × 50 nm³ box, For the PM6:L8-BO-X blend film, 56 PM6 molecules and 241 L8-BO-X molecules were randomly placed in a 50 × 50 × 50 nm³ box, while for the PM6:L8-BO-X:DYO-1 blend film, 56 PM6 molecules, 218 L8-BO-X molecules, and 10 DYO-1 molecules were randomly placed in the same box size. All these ratios are consistent with the experimental ratios. All these BHJs films were annealed from 500 K down to 300 K gradually, during 50 ns. The production run lasted 50 ns after an equilibration run of 100 ns. All analyses were conducted based on the production run.

The LINCS algorithm was utilized to constrain covalent bonds involving hydrogen atom.[3] A simulation time step of 1.0 femtoseconds was employed. Both the pressure and temperature were regulated using the Parrinello–Rahman barostat at 1 atm and the Nose–Hoover thermostat,[4,5] respectively. The graphics were processed by the Visual Molecular Dynamics (VMD) program.[6] Analyses of molecular stacking were performed using the MDAnalysi Python library.

The nuclear magnetic resonance (NMR) spectra and High-Resolution Mass Spectra (HR-MS). The $^{1}H/^{13}C$ nuclear magnetic resonance ($^{1}H/^{13}C$ NMR) spectra of all compounds were obtained from a Bruker AV400 Spectrometer. Time of flight mass spectrometer (TOF-MS) was obtained from Bruker Daltonics (AutoflexIII LRF200-CID).

UV-visible (UV-vis) absorption. UV-vis absorption spectra and Variable-temperature UV-vis absorption spectra were recorded on a Cary 5000 UV-vis spectrophotometer.

Electrochemical characterizations. The cyclic voltammetry (CV) was performed on a LK98B II Microcomputer-based Electrochemical Analyzer using a glassy carbon

electrode as the working electrode, a saturated calomel electrode (SCE) as reference electrode, and a Pt wire as the counter electrode. The sample film on working electrode was in an acetonitrile solution of 0.1 mol/L n-Bu_4NPF_6 at a scan rate of 100 mV/s. The ferrocene/ferrocenium was employed as internal reference. The HOMO and LUMO levels were calculated using the following equations: $E_{HOMO} = -(E_{ox} + 4.8 - E_{Fc/Fc^+})$ eV, $E_{LUMO} = -(E_{red} + 4.8 - E_{Fc/Fc^+})$ eV.

Fourier-transform photocurrent spectroscopy EQE (FTPS-EQE). The FTPS-EQE measurement was carried out on an Enlitech FTPS PECT-600 instrument. The optimal devices were used for FTPS-EQE measurement directly.

Atomic force microscopy (AFM). The AFM images were obtained from a Bruker Dimension Icon atomic force microscope by using in tapping mode. The film samples were prepared under the same conditions as those used for device fabrication.

Grazing incidence wide angle X-ray scattering (GIWAXS). The GIWAXS data were obtained at Xeuss 3.0 UHR Diffuse X-ray Scattering Station, Xenocs. The film samples on the Si substrate were prepared under the same conditions as those used for device fabrication.

Measurement of charge carrier mobilities. The hole and electron mobilities were measured by using space-charge-limited current (SCLC) method. Hole mobilities were measured with the device structure of ITO/PEDOT:PSS/active layer/MoO_x/Ag. Electron mobilities were measured with the device structure of ITO/ZnO/active layer/PNDIT-F3N/Ag. The hole and electron mobilities estimated by the following equation: $J = 9\varepsilon_0\varepsilon_r\mu V^2/8d^3$, where J is the current density, ε_0 is the vacuum permittivity, ε_r is the relative dielectric constant, V is the internal voltage in the device, and d is the thickness of the active layer.

Transient photocurrent (TPC) Characterization. TPC measurements were performed on a Molex 180081-4320 with light intensity about 0.5 sun, current dynamics were recorded on a digital oscilloscope (Tektronix MDO4104C). Voltages at open circuit and currents under short circuit conditions were measured over a 1 MΩ and a 50 Ω resistor, respectively.

***E*loss Analysis**. The following equation was used to quantify the E_{loss} of OSCs:

$$E_{loss} = E_g^{PV} - qV_{oc} = \left(E_g^{PV} - qV_{oc}^{SQ}\right) + \left(qV_{oc}^{SQ} - qV_{oc}^{rad}\right) + \left(qV_{oc}^{rad} - qV_{oc}\right) = \Delta E_1 + \Delta E_2 + \Delta E_3$$

E_g^{PV} represents the bandgap of the blend film and q is the elementary charge. E_g^{PV} can be estimated via the derivatives of the sensitive EQE (EQE_{PV}) spectra(P(E)=dEQE/dE) as following:

$$E_g^{PV} = \frac{\int_a^b E_g \mathrm{P}(E_g)\mathrm{d}E_g}{\int_a^b \mathrm{P}(E_g)\mathrm{d}E_g}$$

where the integration limits a and b are chosen as the energy where P(E_g) is equal to 50% of its maximum. The EQE_{PV} measurements were conducted on an Enlitech FTPS PECT-600 instrument. The total E_{loss} can be divided into three parts:

(1) $\Delta E_1 = E_g - qV_{oc}^{SQ}$ represents the unavoidable radiative loss originating from absorption above the bandgap. The V_{oc}^{SQ} is the maximum voltage based on the Shockley–Queisser (SQ) limit:

$$V_{oc}^{SQ} = \frac{kT}{q}\ln\left(\frac{J_{sc}^{SQ}}{J_0^{SQ}} + 1\right) \cong \frac{kT}{q}\ln\left(\frac{q\cdot\int_{E_g}^{+\infty}\phi_{AM1.5G}(E)\mathrm{d}E}{q\cdot\int_{E_g}^{+\infty}\phi_{BB}(E)\mathrm{d}E}\right)$$

(2) $\Delta E_2 = qV_{oc}^{SQ} - qV_{oc}^{rad}$ can be regarded as radiative loss caused by absorption below the bandgap, where the V_{oc}^{rad} is the open circuit voltage when there is only radiative recombination. The radiative recombination limit for the saturation current (J_0^{rad}) is also calculated from the EQE spectrum:

$$V_{oc}^{rad} = \frac{kT}{q}\ln\left(\frac{J_{sc}}{J_0^{rad}} + 1\right) \cong \frac{kT}{q}\ln\left(\frac{q\cdot\int_0^{+\infty}\mathrm{EQE}(E)\phi_{AM1.5G}(E)\mathrm{d}E}{q\cdot\int_0^{+\infty}\mathrm{EQE}(E)\phi_{BB}(E)\mathrm{d}E}\right)$$

where q is the elementary charge and ϕ_{BB} is the black body spectrum at 300 K.

(3) $\Delta E_3 = qV_{oc}^{rad} - qV_{oc}$ can be directly calculated while the other two parts were determined. ΔE_3 can also be confirmed by measuring the EQE of electroluminescence

(EQE_{EL}) of the solar cell through the equation of: $\Delta E_3 = -kT \ln(EQE_{EL})$. For the EQE_{EL} measurements, a digital source meter (Keithley 2400) was 80 employed to inject electric current into the solar cells, and the emitted photons were collected by a Si diode (Hamamatsu s1337-1010BQ) and indicated by a picoammeter (Keithley 6482).

The transient absorption spectroscopy (TAS). The transient absorption spectrometer utilized in this study was a femtosecond system. A femtosecond laser amplifier (Spectra-Physics) generated an 800 nm pulse at a frequency of 1 kHz, which was then split into two beams to produce the pump and probe pulses, respectively. The probe pulses were focused onto a 3 mm sapphire crystal and 8 mm YAG to generate visible light (450–800 nm) and infrared light (850−1300 nm). To control the time delay between the pump and probe pulses, a mechanical delay stage was employed. The pump pulse was modulated by a mechanical chopper operating at 500 Hz and then focus on the fixed sample together with probe beams. The probe beam was collected into a fiber-coupled spectrometer. The energy of the pump pulse was measured using a power meter (PM400, Thorlabs). The beam size of the pump pulse was measured using a beam profiler (BC106N-VIS/M, Thorlabs).

4. Supporting Figures and Tables

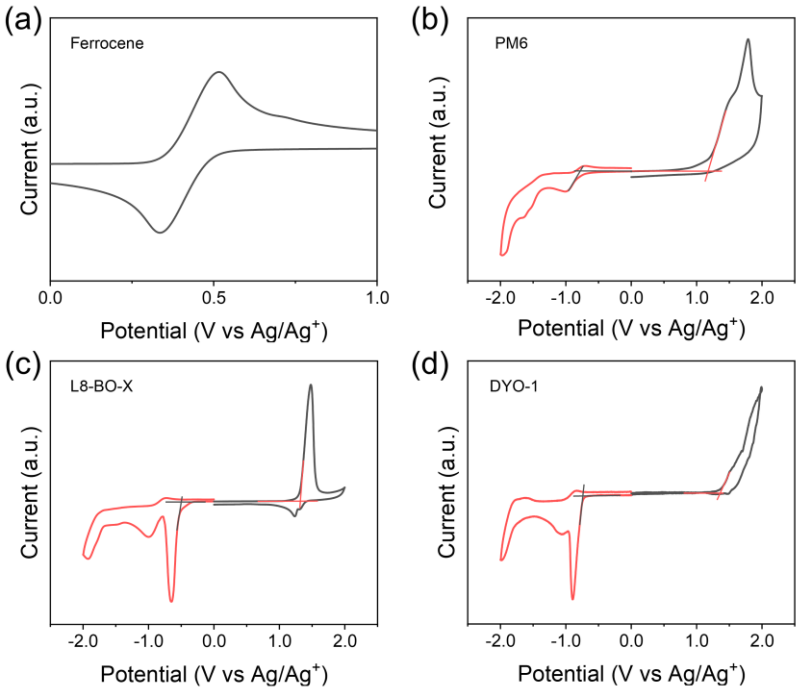

Figure S1. Cyclic voltammetry (CV) plots of (a) reference (ferrocene), (b) PM6 film, (c) L8-BO-X film, and (d) DYO-1 film.

Table S1. The photophysical and electrochemical properties of DYO-1.

Molecule	$\lambda_{max}^{sol.}$ **(nm)**	λ_{max}^{film} **(nm)**	E_g^{opt} **(eV)**	E_{LUMO}^{cv} **(eV)**	E_{HOMO}^{cv} **(eV)**
DYO-1	713	755	1.52	-3.64	-5.75

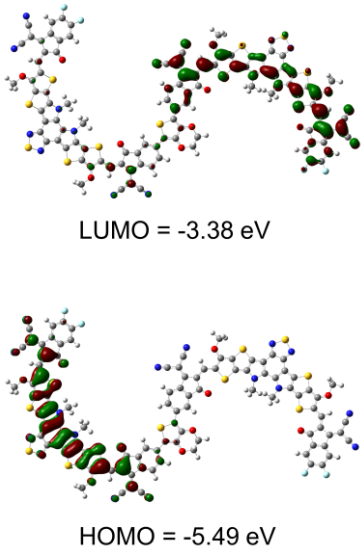

Figure S2. Calculated FMOs and HOMO/LUMO levels of DYO-1.

Table S2. Process optimization of PM6:DYO-1 based binary devices.

D:A	Solvent	Additive	TA	V_{oc} (V)	*FF* (%)	J_{sc} (mA cm^{-2})	PCE (%)
1:0.8	*o*-XY	/	/	1.027	56.5	18.0	10.7
1:1.0				1.029	60.2	18.7	11.6
1:1.2				1.030	61.2	19.3	12.2
1:1.4				1.031	56.0	19.3	11.1
1:1.2	*o*-XY	50% 2-MN	90℃/5 min	1.025	72.4	19.5	14.6
		75% 2-MN		1.023	73.8	19.6	15.0
		100% 2-MN		1.022	73.9	19.8	15.1
		125% 2-MN		1.014	73.2	20.0	15.0

Table S3. Process optimization of PM6:L8-BO-X based binary devices.

D:A	Solvent	Additive	TA	V_{oc} (V)	*FF* (%)	J_{sc} (mA cm^{-2})	PCE (%)
1:0.8	*o*-XY	/	/	0.837	73.9	23.4	14.5
1:1.0				0.840	75.6	24.2	15.5
1:1.1				0.844	75.8	24.5	15.7
1:1.2				0.848	74.8	24.1	15.4
1:1.1	*o*-XY	0.20% DIO	90℃/5 min	0.866	77.8	25.3	17.0
		0.35% DIO		0.863	78.6	26.1	17.6
		0.50% DIO		0.859	77.6	25.8	17.1
		0.70% DIO		0.854	75.2	24.8	15.9

Table S4. Process optimization of PM6:L8-BO-X:DYO-1 based ternary devices.

D:A	Solvent	Additive	TA	V_{oc} (V)	*FF* (%)	J_{sc} (mA cm^{-2})	PCE (%)
1:1.1:0.1	*o*-XY	/	/	0.888	73.4	25.6	16.7
1:1.1:0.2				0.890	71.3	24.6	15.6
1:1:0.1				0.891	73.5	25.7	16.9
1:1:0.2				0.898	73.1	25.0	16.5
1:0.9:0.2				0.907	73.0	24.5	16.3
1:1:0.1	*o*-XY	/	90℃/5 min	0.903	75.6	25.8	17.6
1:1:0.1	*o*-XY	0.20% DIO	90℃/5 min	0.874	79.5	26.6	18.5
		0.35% DIO		0.882	79.8	27.8	19.6
		0.50% DIO		0.863	79.0	26.9	18.4
		0.70% DIO		0.854	75.9	26.3	17.1

Table S5. Summary of the dimer-based binary OSCs with high V_{oc} reported in the literatures.

Active layer	V_{oc} (V)	*FF* (%)	J_{sc} (mA cm^{-2})	PCE (%)	Ref.
PM6:*d*T9TBO	0.99	62.1	9.5	5.8	*Angew. Chem. Int. Ed.*, 2023, **62**(21), e202303066
PM6:2BOHD-T	0.95	24.9	75.0	17.7	*Nano Energy*, 2024, **121**, 109218
PM6:2BOHD-TC$_4$T	0.98	73.8	22.8	16.5	
PM6:2BOHD-TC$_6$T	0.98	70.6	21.9	15.1	
PM6:DY-3T	0.97	72.6	22.9	16.1	*Macromol. Rapid Commun.*, 2024, 2400433
PM6:DY-TVCl	0.93	75.3	25.7	18.0	
PM6:EV-o	0.96	42.1	6.2	2.5	*Angew. Chem. Int. Ed.*, 2023, **62**(26), e202303551
PM6:D-TPh	0.95	78.7	25.6	19.1	*Angew. Chem. Int. Ed.*, 2024, **63**(50), e202411044
PM6:D-TN	0.93	78.2	25.3	18.4	
PM6:T0	0.92	77.1	24.1	17.1	*Adv. Mater.*, 2024, **36**(35), 2403890
PM6:T1	0.96	71.7	21.2	14.6	
PM6:T4	0.96	76.6	22.5	16.6	
PM6:T6	0.97	76.8	22.9	17.1	
PM6:T12	0.98	70.9	21.3	14.8	
D18:DYF-V	0.93	0.7	16.0	10.0	*Adv. Funct. Mater.*, 2024, **34**(41), 2406501
D18:DYF-E	0.94	0.8	24.2	17.0	
D18:DYTVT	0.97	74.0	24.1	17.4	*Adv. Funct. Mater.*, 2024, **34**(39), 2404569
D18:DYTCVT	0.94	76.0	23.7	17.0	
PBQx-H-TF/dBTIC-δV-BO	0.96	66.1	20.7	13.2	*Adv. Funct. Mater.*, 2024, **34**(1), 2305608
PBQx-H-TF/dBTIC-γV-BO	0.91	76.6	24.5	17.1	
PM6:CH-D1	0.95	73.2	23.9	16.6	*Adv. Energy Mater.*, 2023, **13**(20), 2300301
PM6:CH8-0	0.94	72.1	22.6	15.3	*Energy Environ. Sci.*, 2023,**16**(4), 1773-1782
PM6:CH8-1	0.92	74.2	24.9	17.1	
PM6:CH8-2	0.93	74.9	24.2	16.8	
PM6:CH8-3	0.92	77.0	24.4	17.2	*Angew. Chem. Int. Ed.*, 2023, **62**(38), e202307962
PM6:CH8-5	0.90	75.2	24.8	16.8	
PM6:DYBO	0.97	75.8	24.6	18.1	*Joule*, 2023, **7**(2), 416-430.
D18:DP-BTP	0.96	69.1	22.7	15.1	*Angew. Chem. Int. Ed.*, 2024, **63**(1), e202316039
PM6:DYT	0.94	76.0	24.1	17.3	*ACS Energy Lett.*, 2023, **8**(3), 1344-1353.
PM6:DYV	0.93	78.0	25.6	18.6	
PM6:DYTVT	0.95	74.0	24.8	17.7	
PM6:Dimer-Qx	0.93	69.3	22.6	14.6	

PM6:Dimer-2CF	0.90	80.0	26.4	19.0	*Adv. Mater.*, 2024, **36**(4), 2310046
PM6:2-BTP-2F-T	0.91	78.3	25.5	18.2	*Adv. Sci.*, 2022, **9**(23), 2202513.
PM6:DIBP3F-Se	0.92	76.1	25.9	18.1	*Angew. Chem. Int. Ed.*, 2023, **62**(45), e202302888
PM6:DIBP3F-S	0.90	72.0	24.9	16.1	
D18:DY-T	0.95	72.5	22.6	15.5	*CCS Chem.*, 2023, **5**(11), 2576-2588
D18:DY-TF	0.95	72.9	24.4	16.8	
D18:DYF-TF	0.94	75.3	25.8	18.3	
D18:DYA-I	0.94	78.0	25.7	18.8	*Adv. Energy Mater.*, 2023, **13**(34), 2301283
D18:DYA-IO	0.95	76.0	24.3	17.5	
D18:DYA-O	0.96	73.0	23.3	16.5	
D18/DY-IT	0.94	73.9	26.0	18.1	*Angew. Chem. Int. Ed.*, 2024, e202418439
D18/DYO-IT	1.01	63.8	22.4	14.4	
D18/DY-FT	0.93	68.6	23.8	15.3	*ACS Energy Lett.*, 2024, **9**(11), 5541−5549
D18/DY-IDT	0.98	64.1	19.1	12.0	
PM6:DYO-1	1.02	73.9	19.8	15.1	*This work*

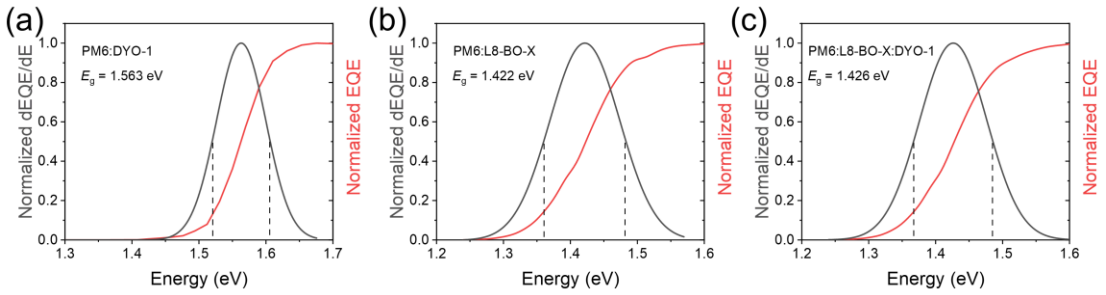

Figure S3. Optical bandgap determination of (a) PM6:DYO-1, (b) PM6:L8-BO-X, (c) PM6:L8-BO-X:DYO-1 based on the derivatives of the EQE spectra. The region between two lines is the part where the gap distribution probability is greater than half of the maximum, which is used for the bandgap calculation.

Table S6. Detail data of energy loss for OSCs.

Active layer	V_{oc} (V)	E_g^{PV} (eV)	ΔE_1 (eV)	ΔE_2 (eV)	$\Delta E_3{}^a$ (eV)	$\Delta E_3{}^b$ (eV)	E_{loss} (eV)
PM6:DYO-1	1.022	1.563	0.277	0.057	0.207	0.238	0.541
PM6:L8-BO-X	0.862	1.422	0.265	0.063	0.232	0.258	0.560
PM6:L8-BO-X:DYO-1	0.881	1.426	0.266	0.061	0.219	0.244	0.545
D18:DYO-1	1.042	1.565	0.277	0.054	0.192	0.218	0.523
D18-Cl:DYO-1	1.069	1.565	0.277	0.053	0.166	0.208	0.496

[a] Calculated from $qV_{oc}^{rad} - qV_{oc}$.

[b] Calculated from $-kT\ln(EQE_{EL})$.

Table S7. Process optimization of D18:DYO-1 and D18-Cl:DYO-1 based binary devices.

Donor	D:A	Solvent	Additive	TA	HTL	V_{oc} (V)	*FF* (%)	J_{sc} (mA cm^{-2})	PCE (%)
D18	1:1.1	CF	/	/	PEDOT:PSS	1.043	60.1	18.0	11.3
	1:1.2					1.052	65.2	17.5	12.1
	1:1.3					1.059	63.9	17.6	11.9
	1:1.2	CF	0.30% 1-MN	90℃/5 min	PEDOT:PSS	1.051	62.1	18.2	11.9
			0.50% 1-MN			1.042	64.5	18.6	12.6
			0.70% 2-MN			1.040	62.8	18.5	12.1
D18-Cl	1:1.2	CF	/	/	PEDOT:PSS	1.072	55.3	15.0	9.0
			0.50% 1-MN	90℃/5 min	PEDOT:PSS	1.067	58.8	16.1	10.2

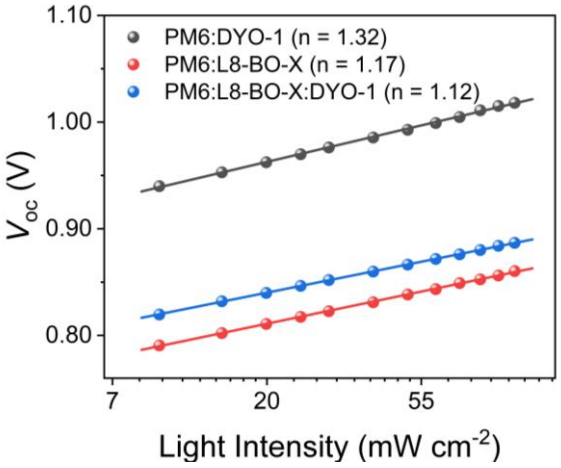

Figure S4. V_{oc} versus light intensity of the binary and ternary devices.

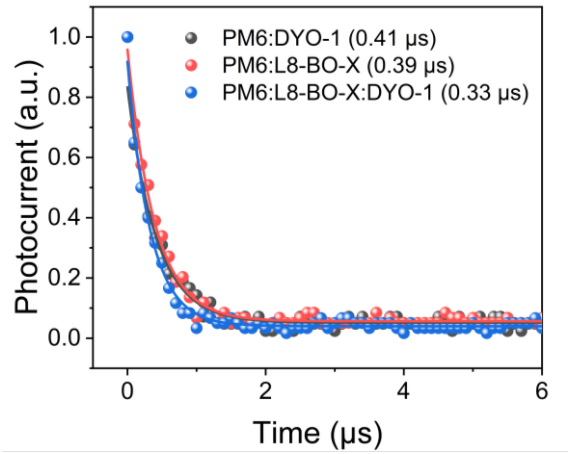

Figure S5. Transient photocurrent (TPC) measurements of OSCs.

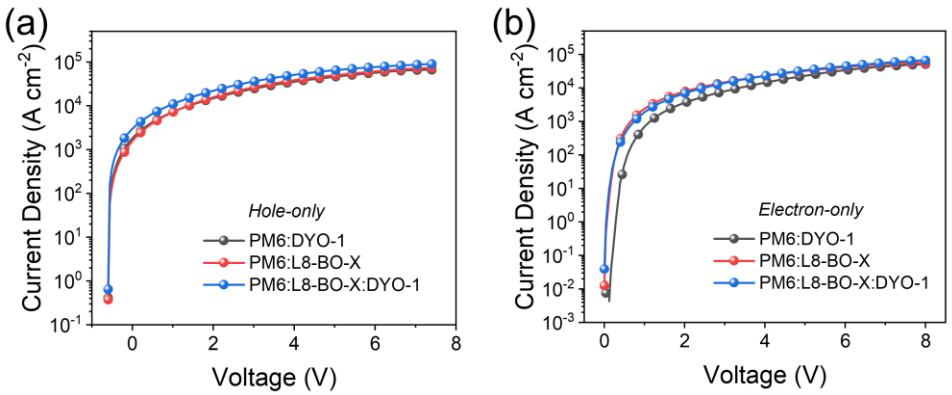

Figure S6. The (a) hole and (b) electron mobility curves based on hole-only and electron-only devices.

Table S8. The hole mobilities and electron mobilities of the binary and ternary devices.

Active layer	μ_h ($\times10^{-4}$ cm^{-2} V^{-1} s^{-1})	μ_e ($\times10^{-4}$ cm^{-2} V^{-1} s^{-1})	μ_h/μ_e
PM6:DYO-1	6.42	3.07	2.09
PM6:L8-BO-X	7.12	3.98	1.79
PM6:L8-BO-X:DYO-1	7.64	4.72	1.62

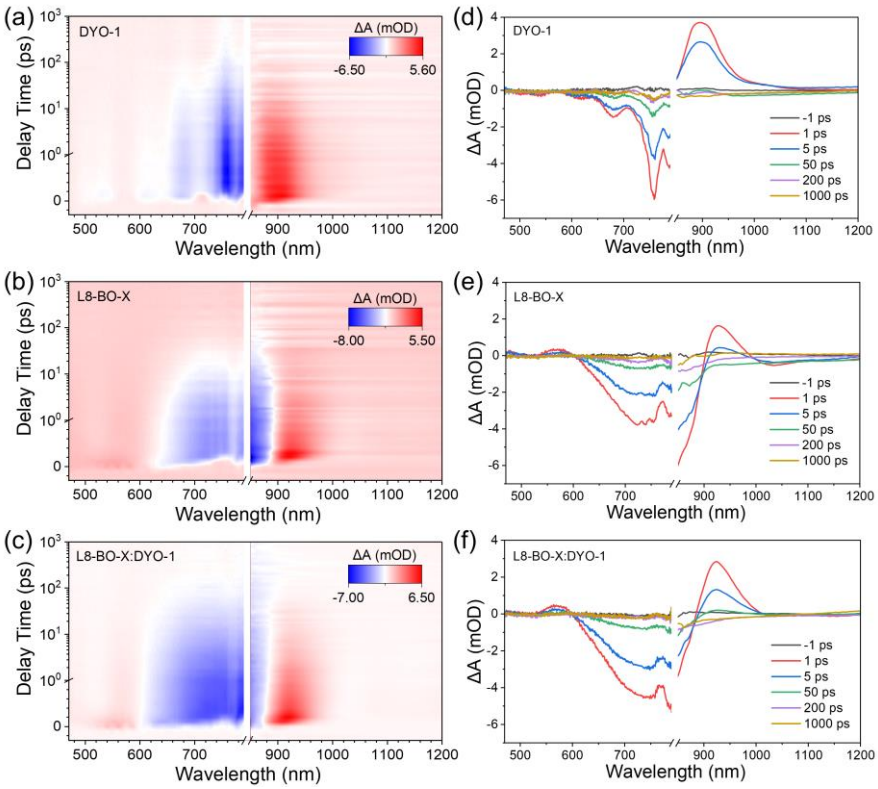

Figure S7. 2D TAS images pumped with 800 nm. (a) Neat DYO-1 film. (b) Neat L8-BO-X film. (c) L8-BO-X:DYO-1 blend film. (d-f) Corresponding TAS at different probe delay times.

Table S9. Detailed fitting parameters at 1030 nm of PM6:L8-BO-X and PM6:L8-BO-X:DYO-1 blend films.

Active layer	A_1 (%)	τ_1 (ps)	A_2 (%)	τ_2 (ps)	τ_{avg} (ps)
PM6:L8-BO-X	0.90	0.91	0.10	12.97	8.30
PM6:L8-BO-X:DYO-1	0.91	0.74	0.09	11.40	7.18

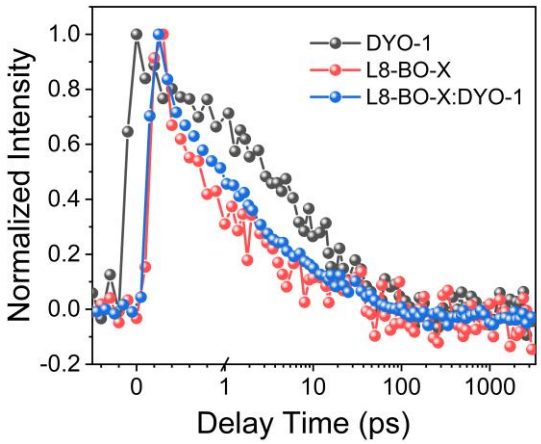

Figure S8. Normalized TAS dynamic curves probed at 930 nm.

Table S10. Summary of the GIWAXS parameters for the PM6:DYO-1, PM6:L8-BO-X, and PM6:L8-BO-X:DYO-1 blend films.

Films	Out-of-Plane π–π stacking				In-Plane Lamellar stacking			
	q (Å^{-1})	*d*-spacing (Å)[a]	FWHM (Å)	CL (Å)[b]	*q* (Å^{-1})	*d*-spacing (Å)[a]	FWHM (Å)	CL (Å)[b]
PM6:DYO-1	1.56	4.04	0.28	20.12	0.29	22.05	0.06	91.21
PM6:L8-BO-X	1.65	3.81	0.18	31.95	0.30	21.01	0.07	79.65
PM6:L8-BO-X:DYO-1	1.62	3.87	0.17	34.27	0.29	21.52	0.07	81.96

[a] Calculated from the equation: *d*-spacing = 2π/*q*.

[b] Obtained from the Scherrer equation: CL = 2 πK/FWHM, where FWHM is the full-width at half-maximum and K is a shape factor (K = 0.9 here).

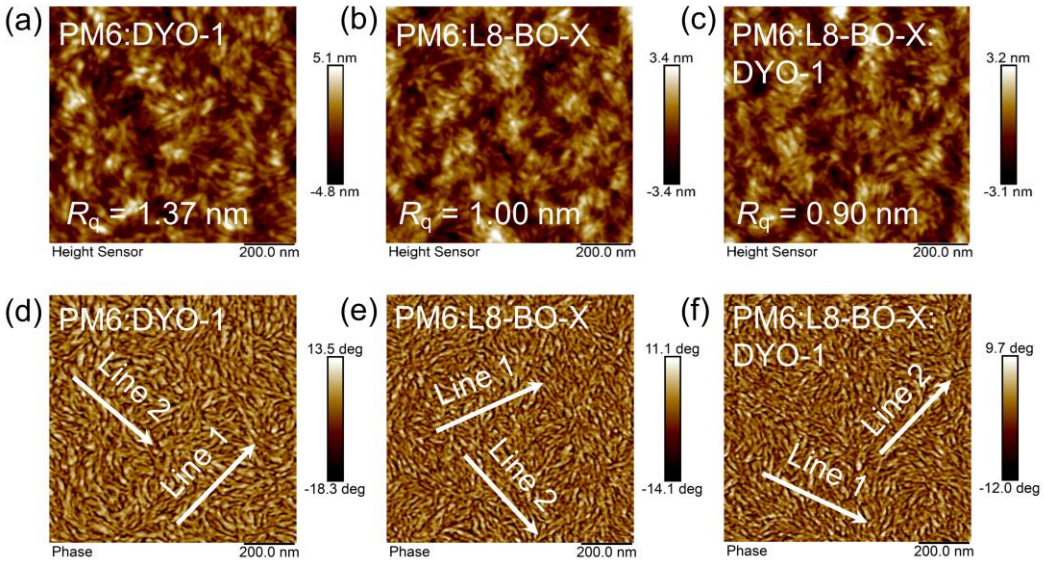

Figure S9. (a-c) AFM height images and (d-f) phase images of the binary and ternary blends.

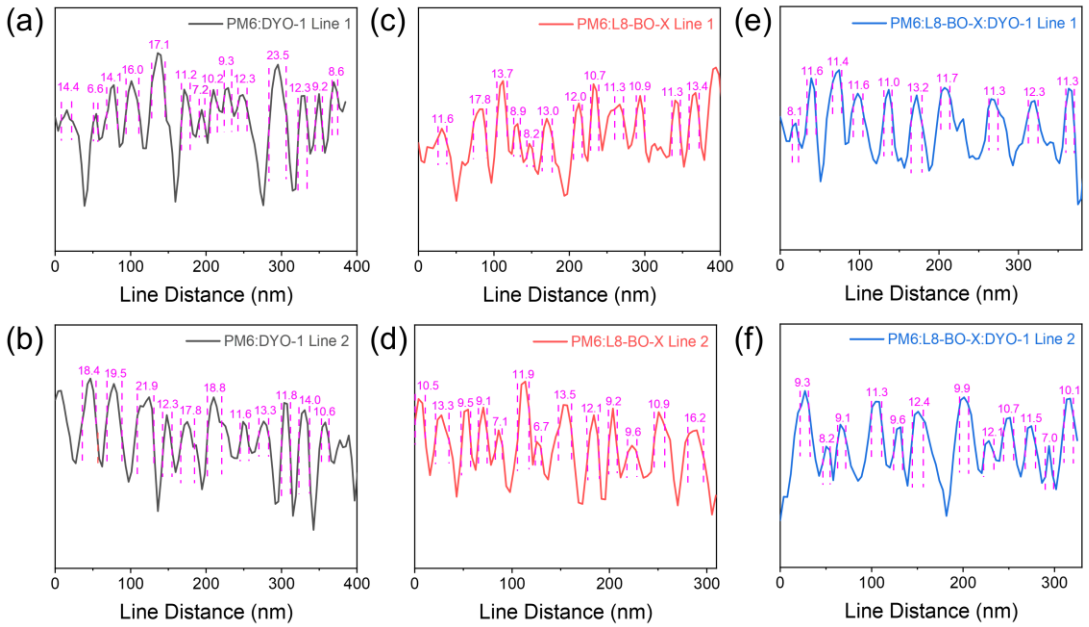

Figure S10. Fibril diameter diagrams of (a-b) PM6:DYO-1, (c-d) PM6:L8-BO-X, and (e-f) PM6:PM6:L8-BO-X:DYO-1 blend films, respectively.

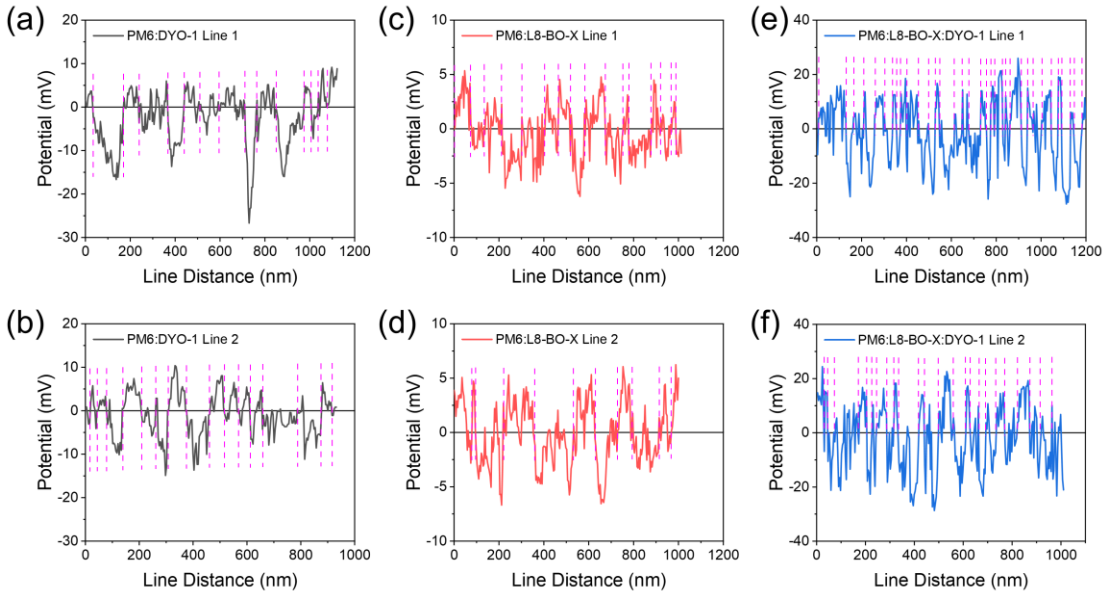

Figure S11. Size analysis of the phase-separated donor:acceptor domains observed from the AFM-IR images of (a-b) PM6:DYO-1, (c-d) PM6:L8-BO-X, and (e-f) PM6:PM6:L8-BO-X:DYO-1 blend films, respectively.

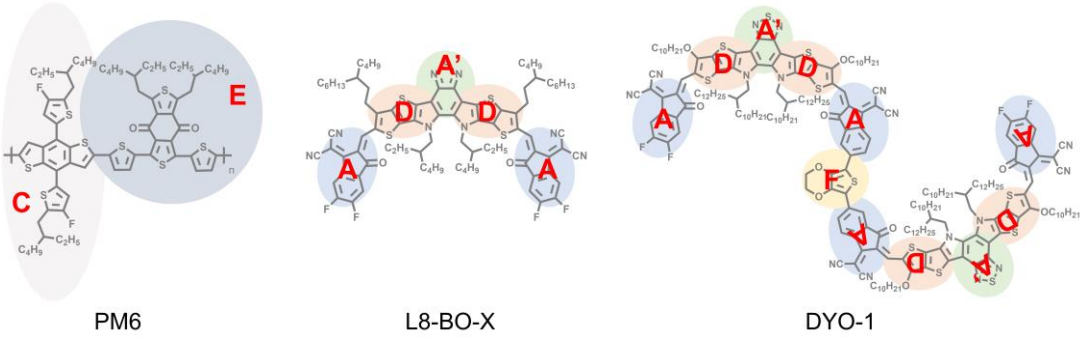

Figure S12. Among PM6, the repeating unit of BDT-F defined as C and the repeating unit of BDD defined as E. For acceptors, the accepter-strong electron end group defined as A, the donor-strong electron group defined as D, the central accepter unit was defined as A' and the central bridge unit in defined as F.

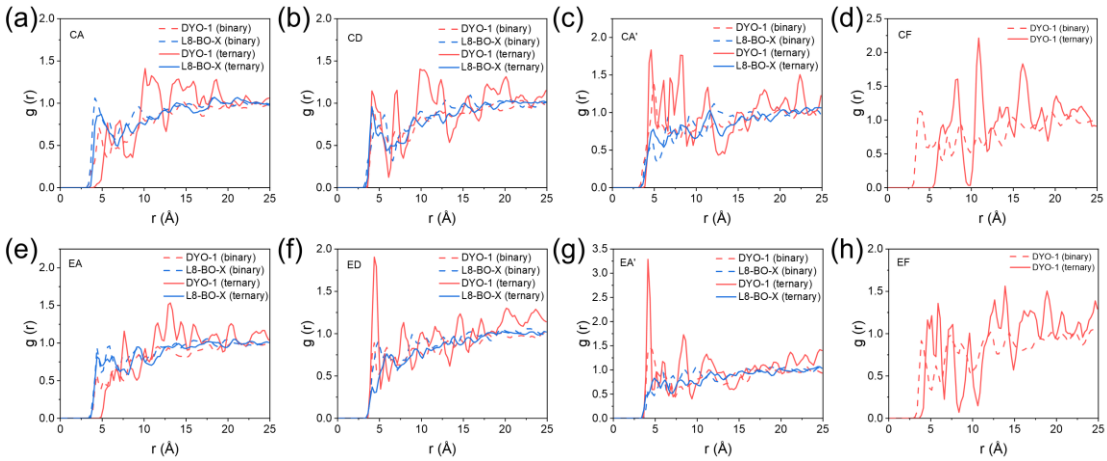

Figure S13. Radial distribution function g (r) for the molecular fragments of PM6, L8-BO-X, and DYO-1 extracted from simulated blends.

Table S11. Total stacking counts per unit volume for PM6:DYO-1, PM6:L8-BO-X, and PM6:L8-BO-X:DYO-1 systems.

BHJ	CA	CD	CA'	EA	ED	EA'	CF	EF	SUM
PM6:L8-BO-X	50.24	28.72	15.16	53.76	36.36	17.60	/	/	201.84
PM6:DYO-1	32.96	20.15	12.63	37.56	25.34	13.34	6.62	7.29	155.89
PM6:L8-BO-X:DYO-1[a]	38.80	21.33	11.69	43.37	24.83	12.94	/	/	152.96
PM6:L8-BO-X:DYO-1[b]	3.68	2.95	1.48	3.47	2.62	1.63	0.54	0.53	16.90

[a] Total stacking counts per unit volume for PM6 and L8-BO-X in the PM6:L8-BO-X:DYO-1 system.
[b] Total stacking counts per unit volume for PM6 and DYO-1 in the PM6:L8-BO-X:DYO-1 system.

Table S12. Face-on stacking counts per unit volume for PM6:DYO-1, PM6:L8-BO-X, and PM6:L8-BO-X:DYO-1 systems.

BHJ	CA	CD	CA'	EA	ED	EA'	CF	EF	SUM
PM6:L8-BO-X	8.67	7.36	3.33	6.73	6.99	3.35	/	/	36.43
PM6:DYO-1	3.57	5.76	2.76	3.02	1.60	3.25	1.53	0.82	22.31
PM6:L8-BO-X:DYO-1[a]	6.31	5.45	2.55	5.23	4.90	2.53	/	/	26.97
PM6:L8-BO-X:DYO-1[b]	0.21	0.60	0.38	1.60	0.70	0.50	0.00	0.90	4.89

[a] Face-on stacking counts per unit volume for PM6 and L8-BO-X in the PM6:L8-BO-X:DYO-1 system.
[b] Face-on stacking counts per unit volume for PM6 and DYO-1 in the PM6:L8-BO-X:DYO-1 system.

5. Spectral Charts of NMR

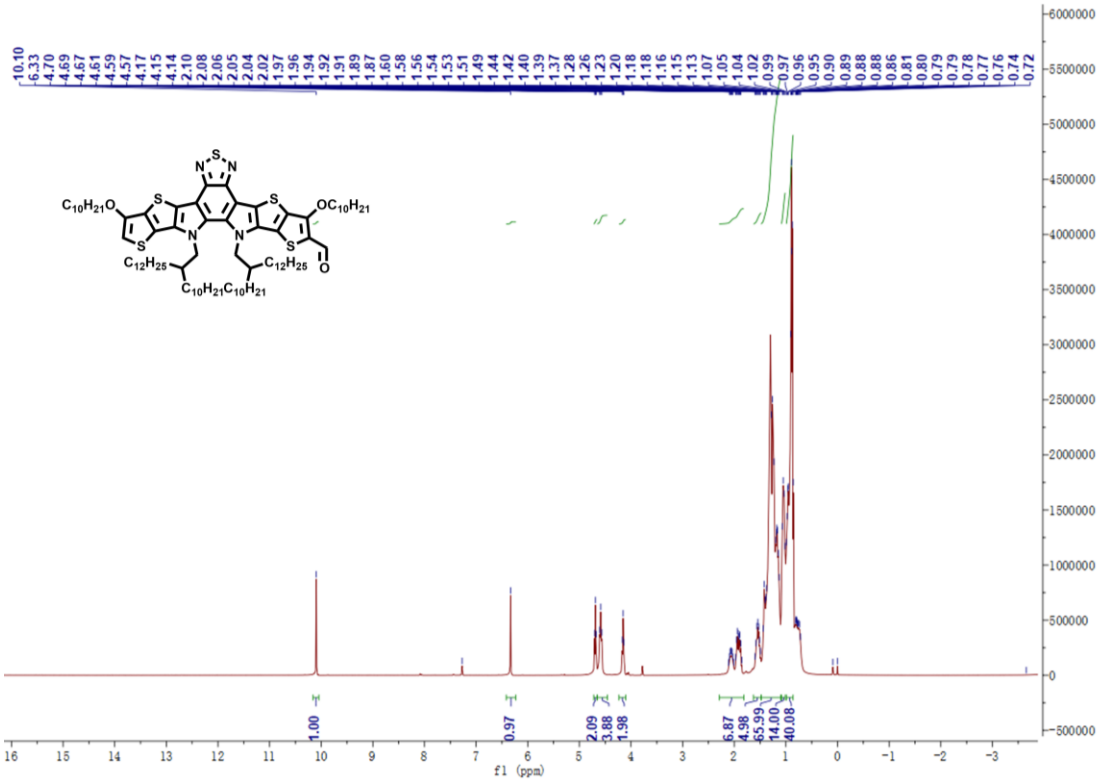

Figure S14. ^{1}H NMR spectrum of compound 2 at 300K in $CDCl_3$.

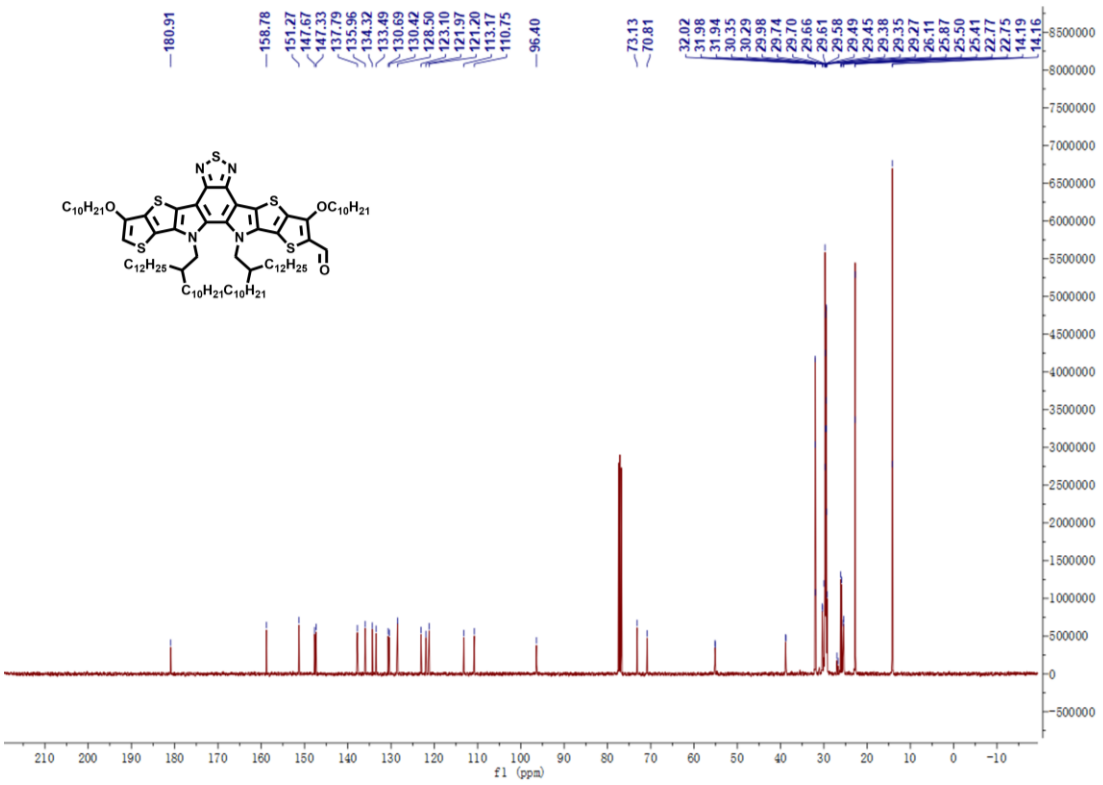

Figure S15. ^{13}C NMR spectrum of compound 2 at 300K in $CDCl_3$.

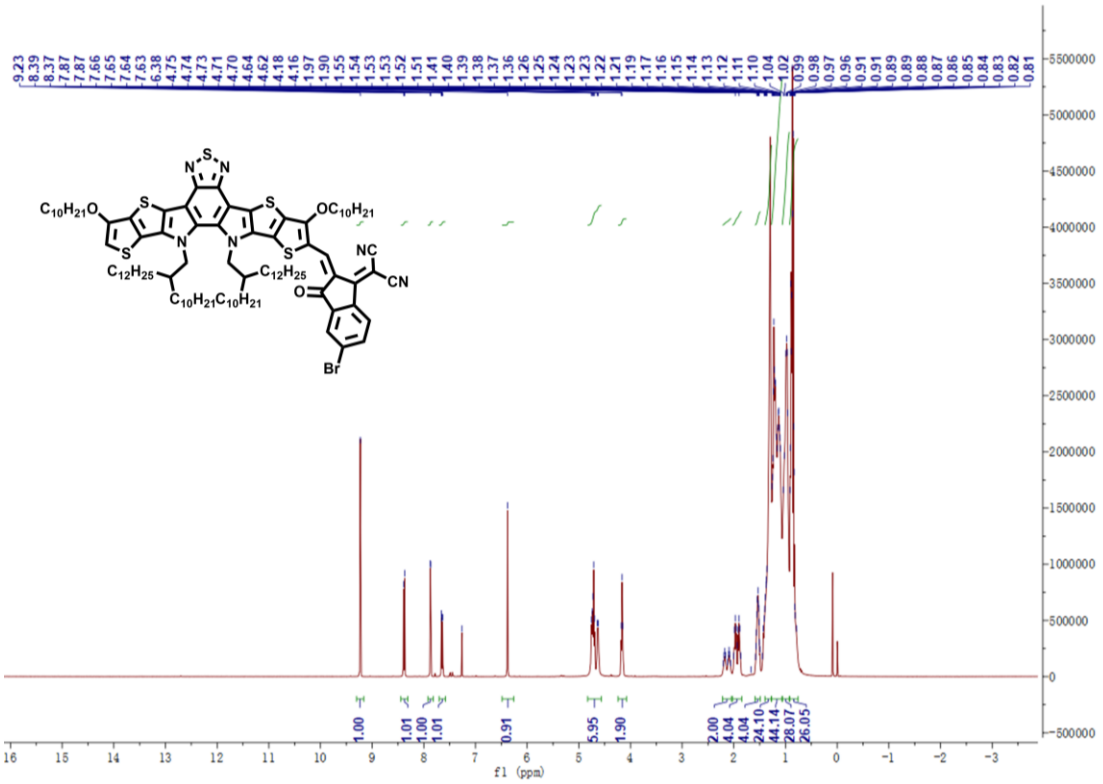

Figure S16. ^{1}H NMR spectrum of compound 3 at 300K in $CDCl_3$.

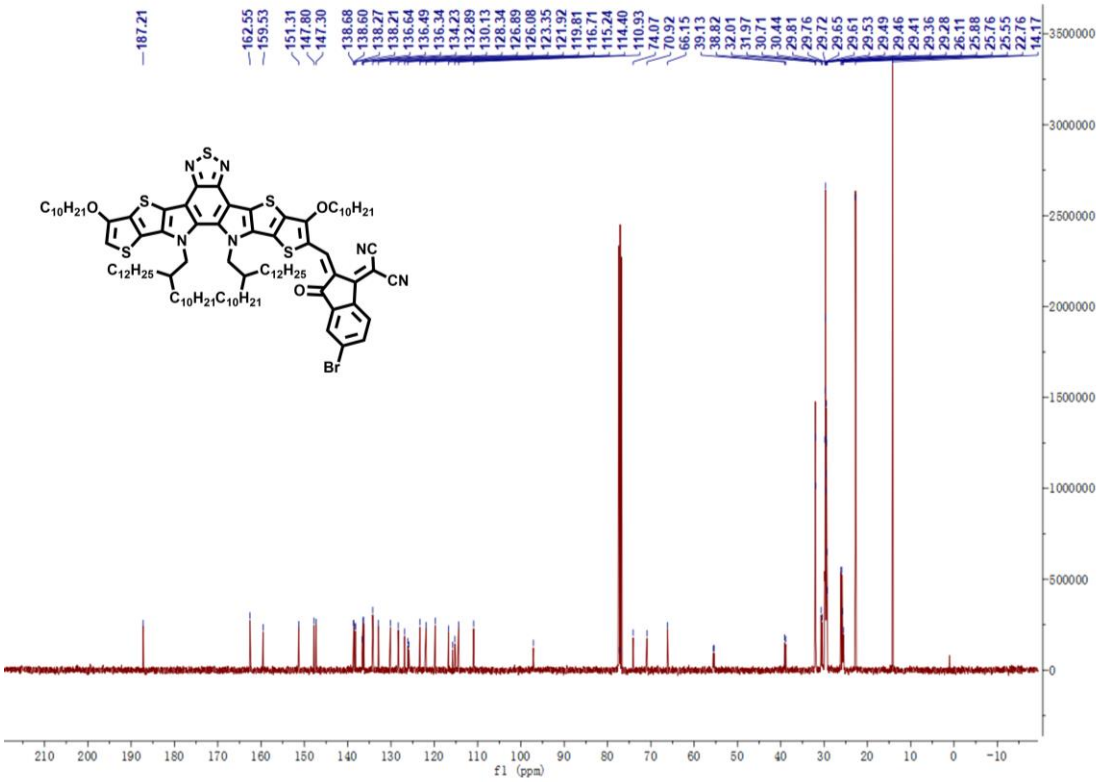

Figure S17. ^{13}C NMR spectrum of compound 3 at 300K in $CDCl_3$.

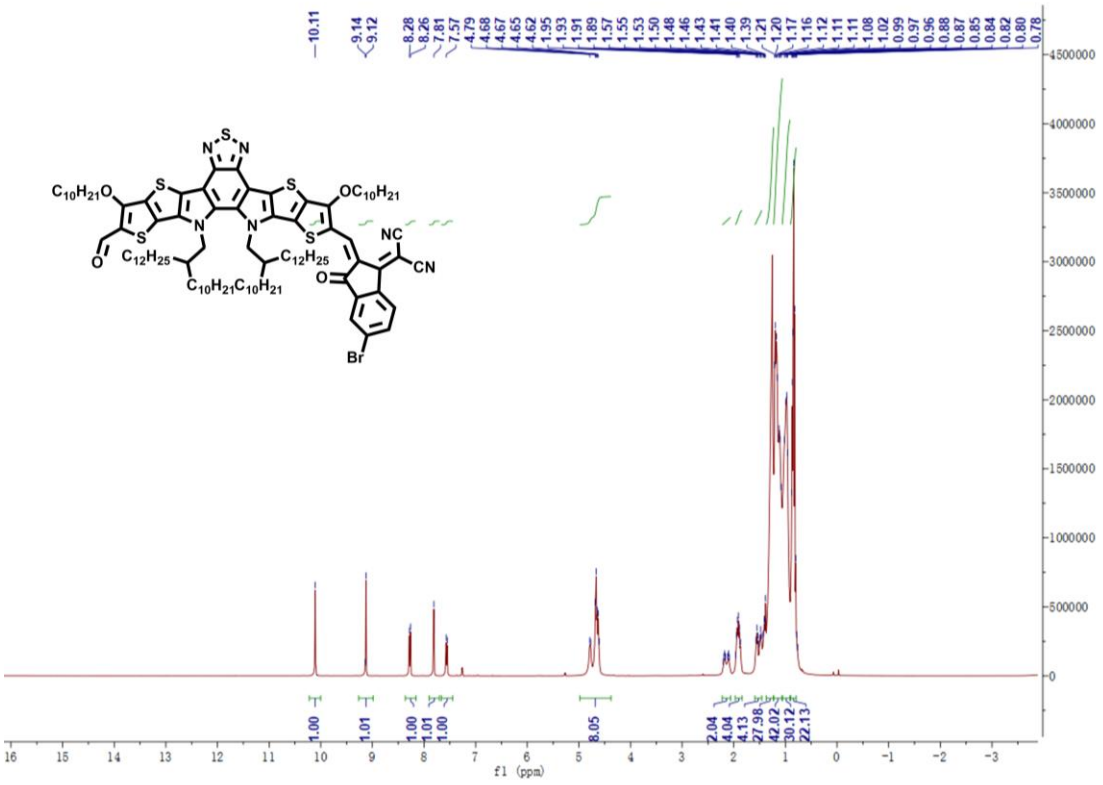

Figure S18. ^{1}H NMR spectrum of compound 4 at 300K in $CDCl_3$.

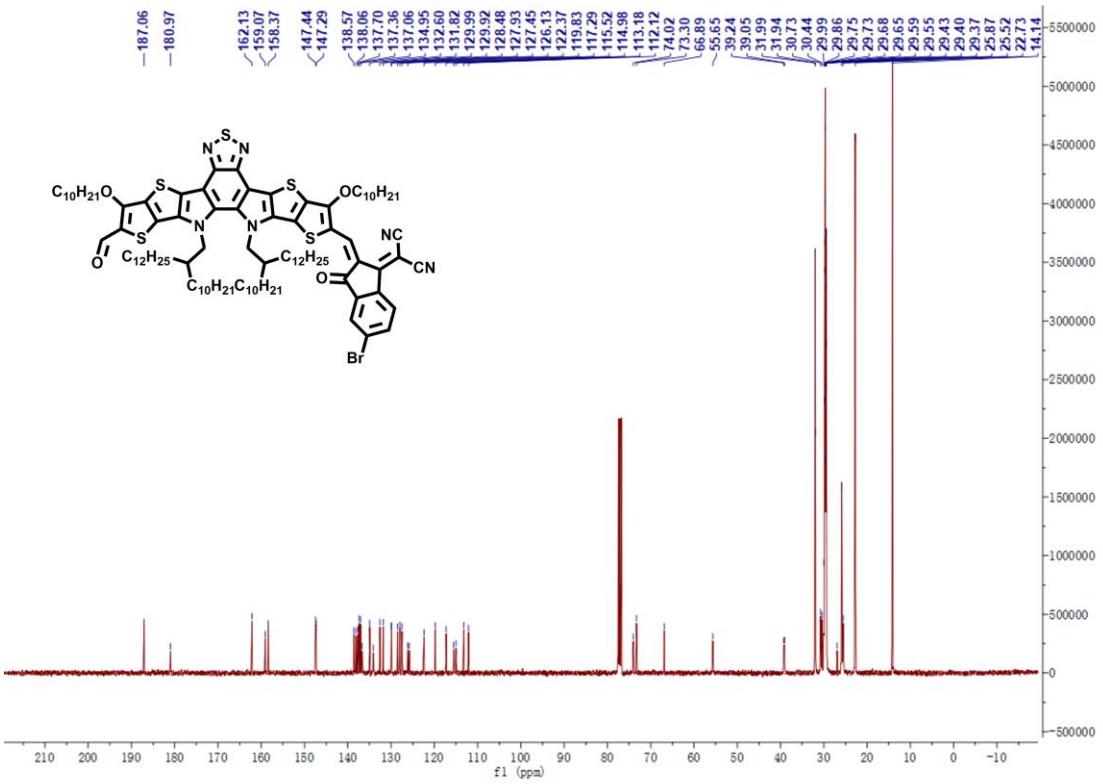

Figure S19. ^{13}C NMR spectrum of compound 4 at 300K in $CDCl_3$.

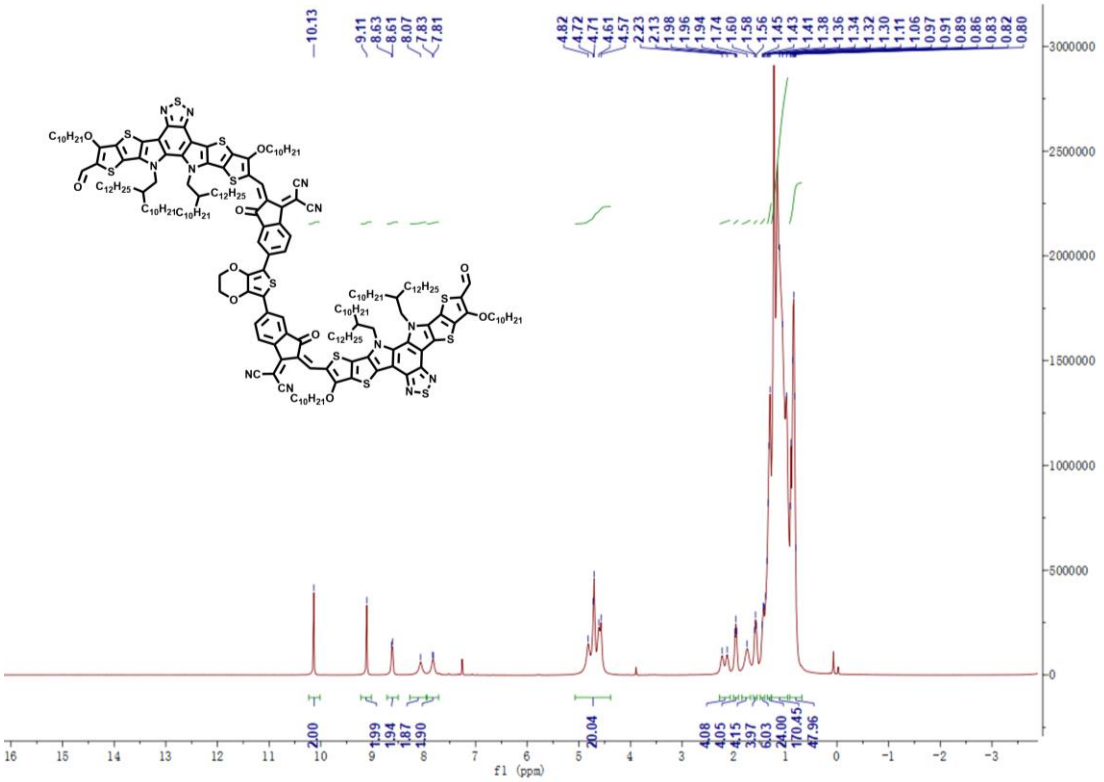

Figure S20. ^{1}H NMR spectrum of compound 5 at 300K in $CDCl_3$.

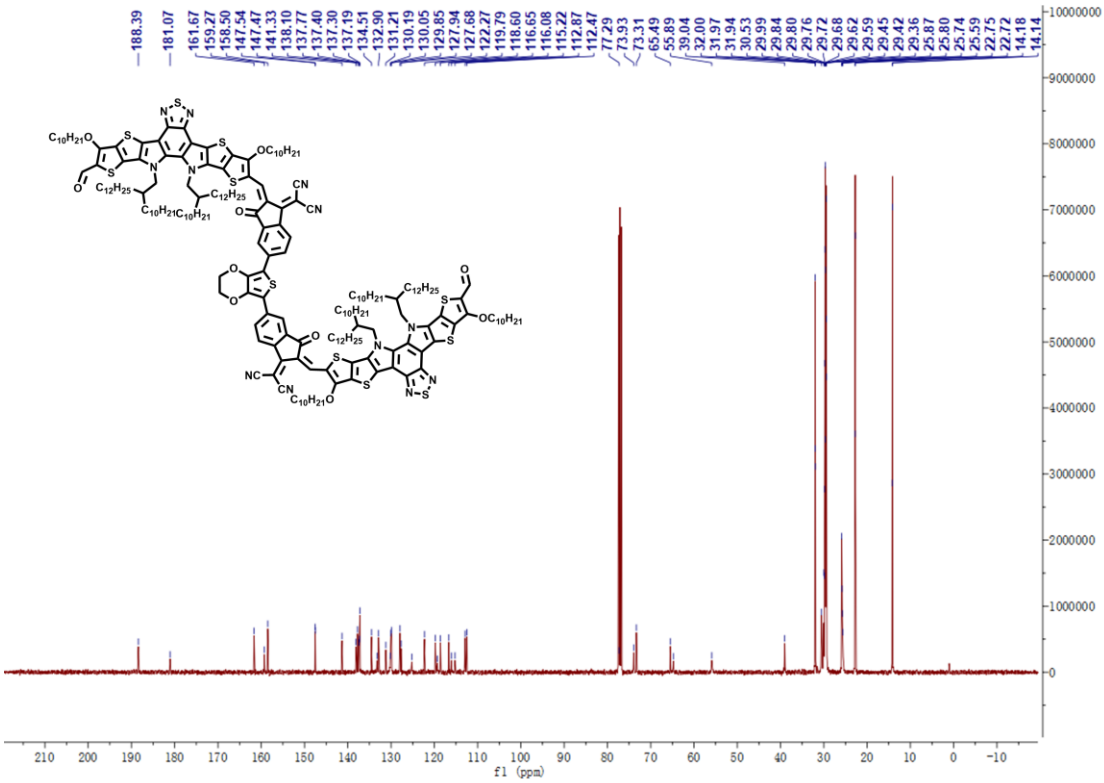

Figure S21. ^{13}C NMR spectrum of compound 5 at 300K in $CDCl_3$.

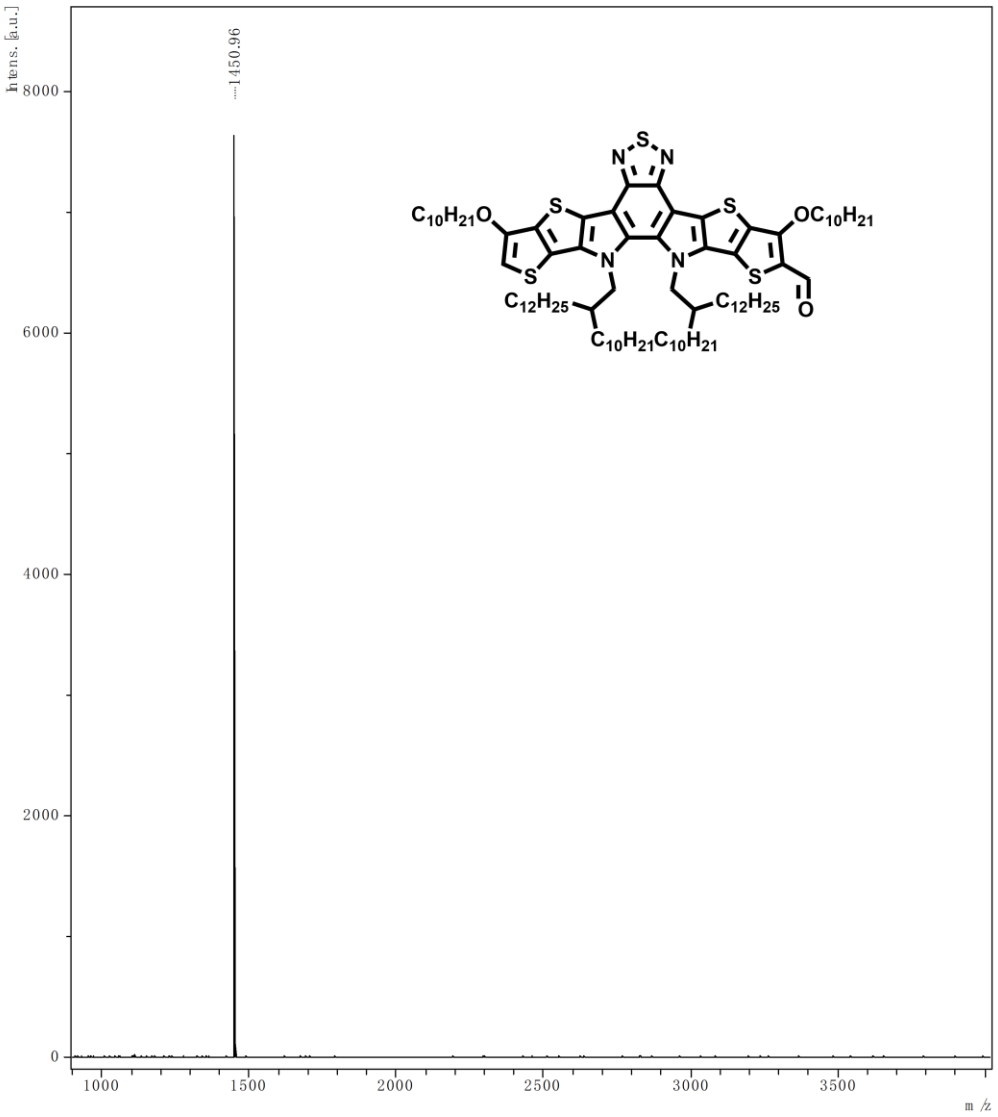

Figure S22. MS of Compound 2.

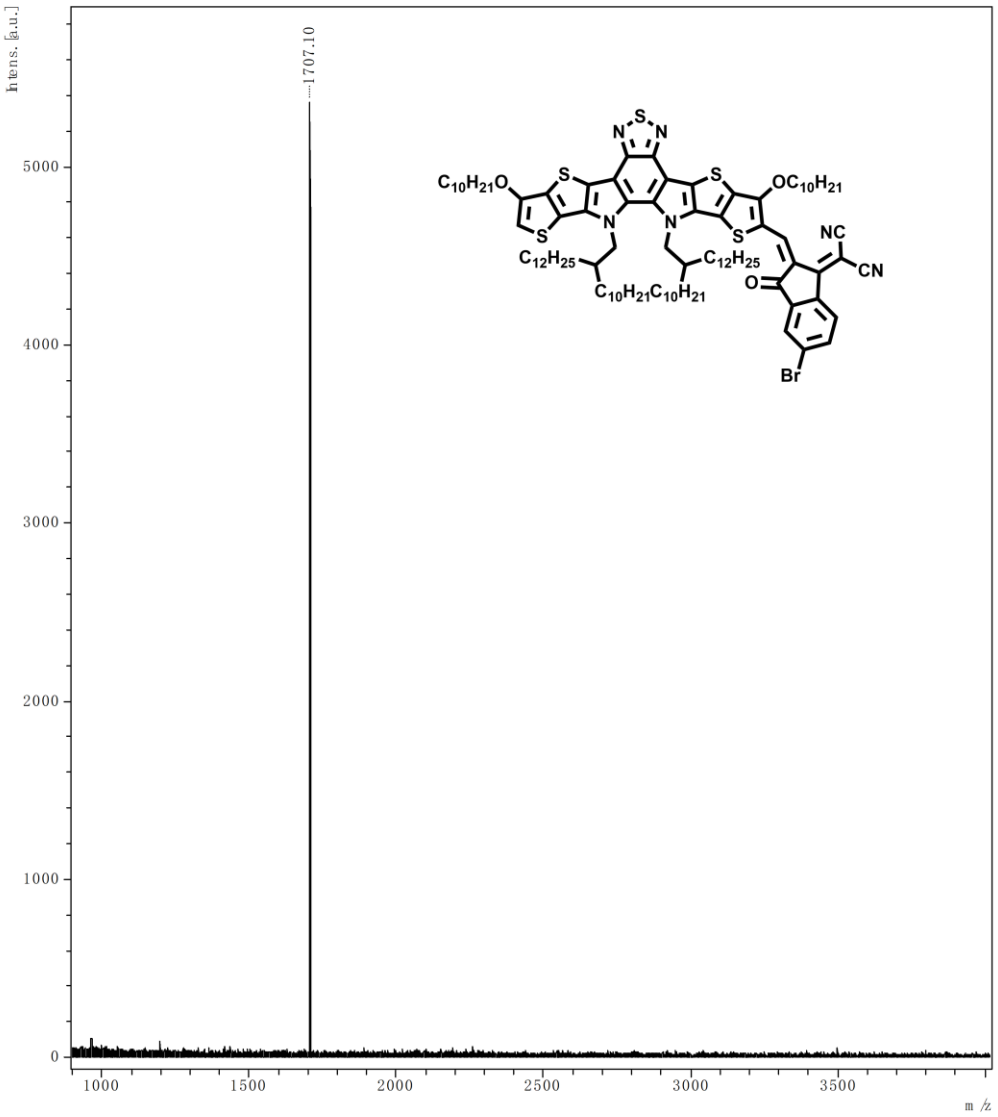

Figure S23. MS of Compound 3.

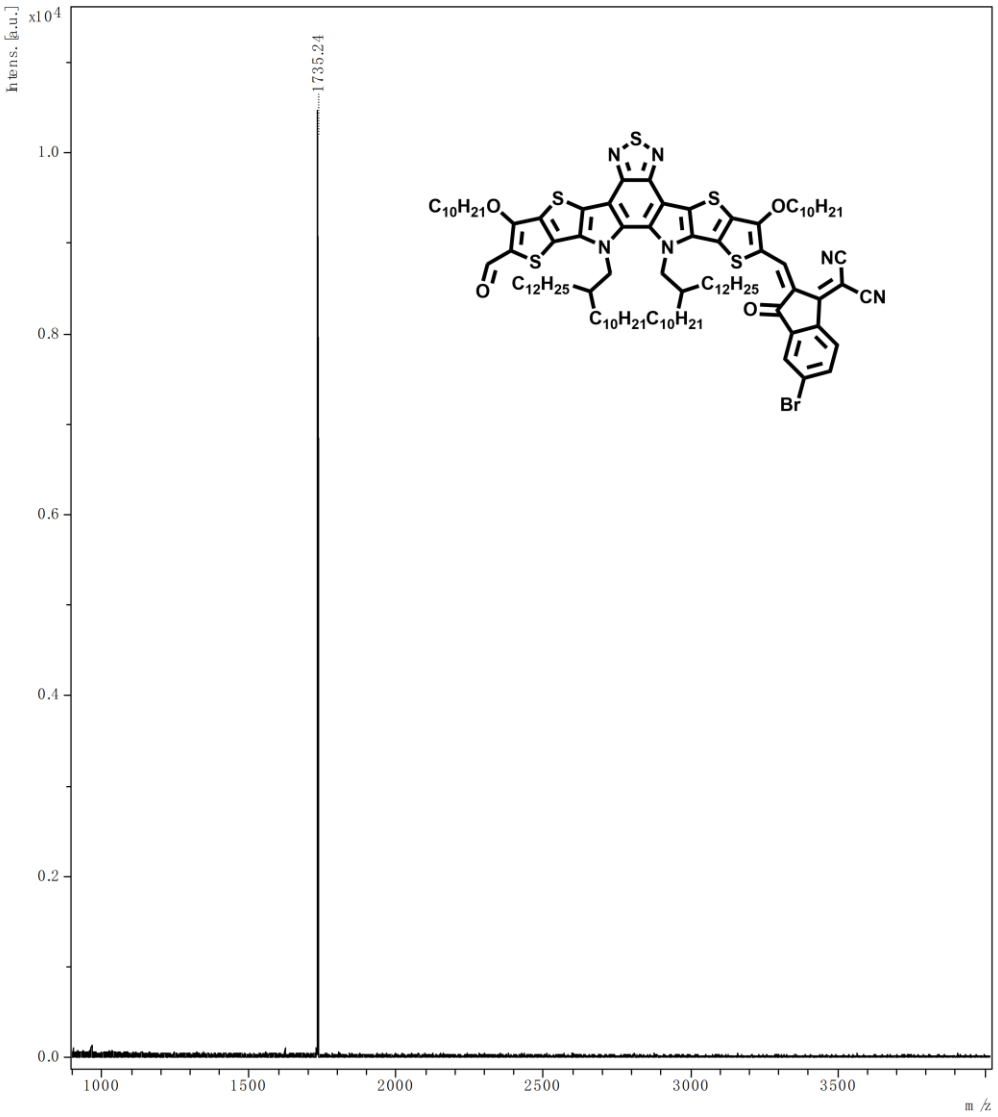

Figure S24. MS of Compound 4.

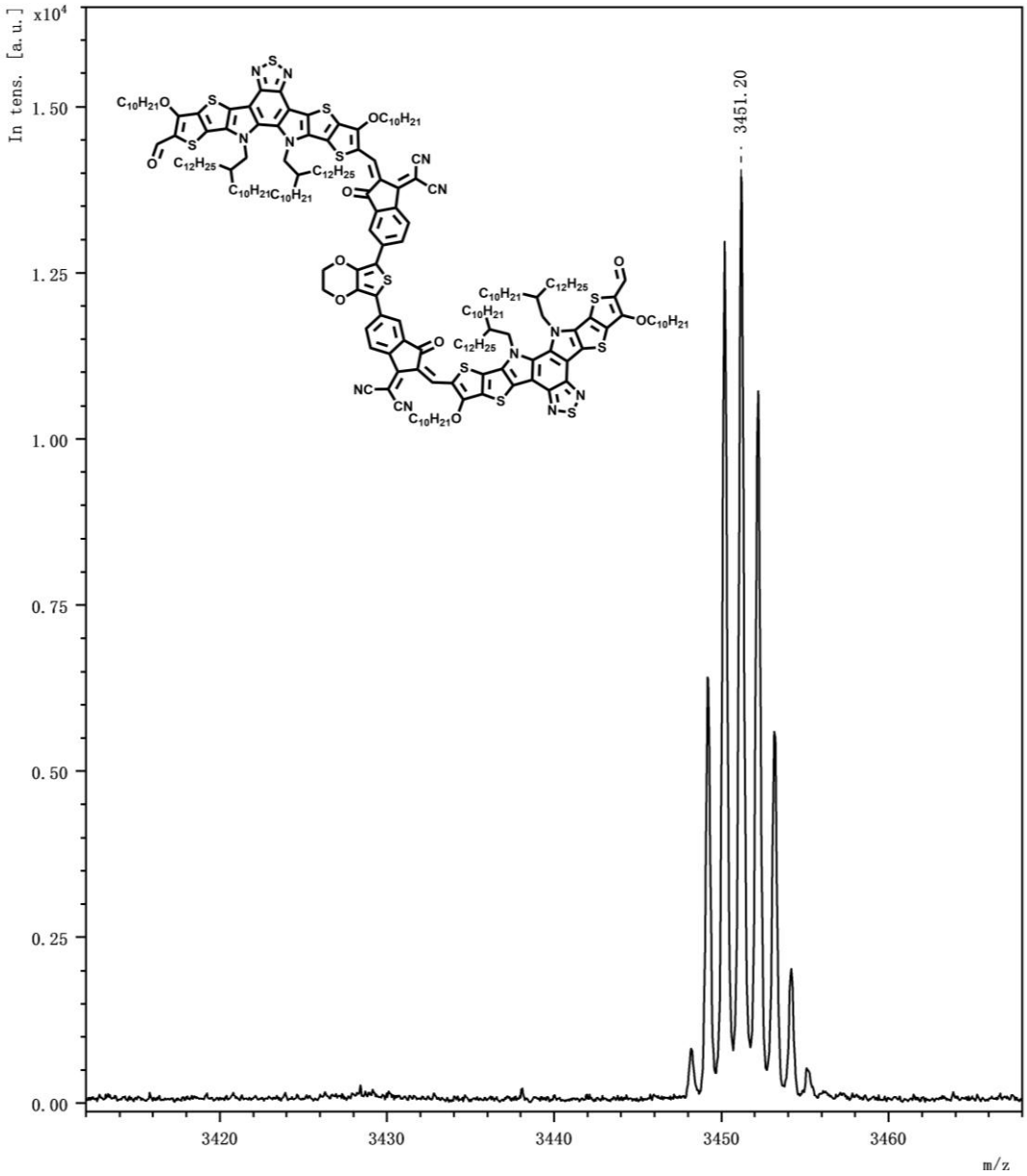

Figure S25. MS of Compound 5.

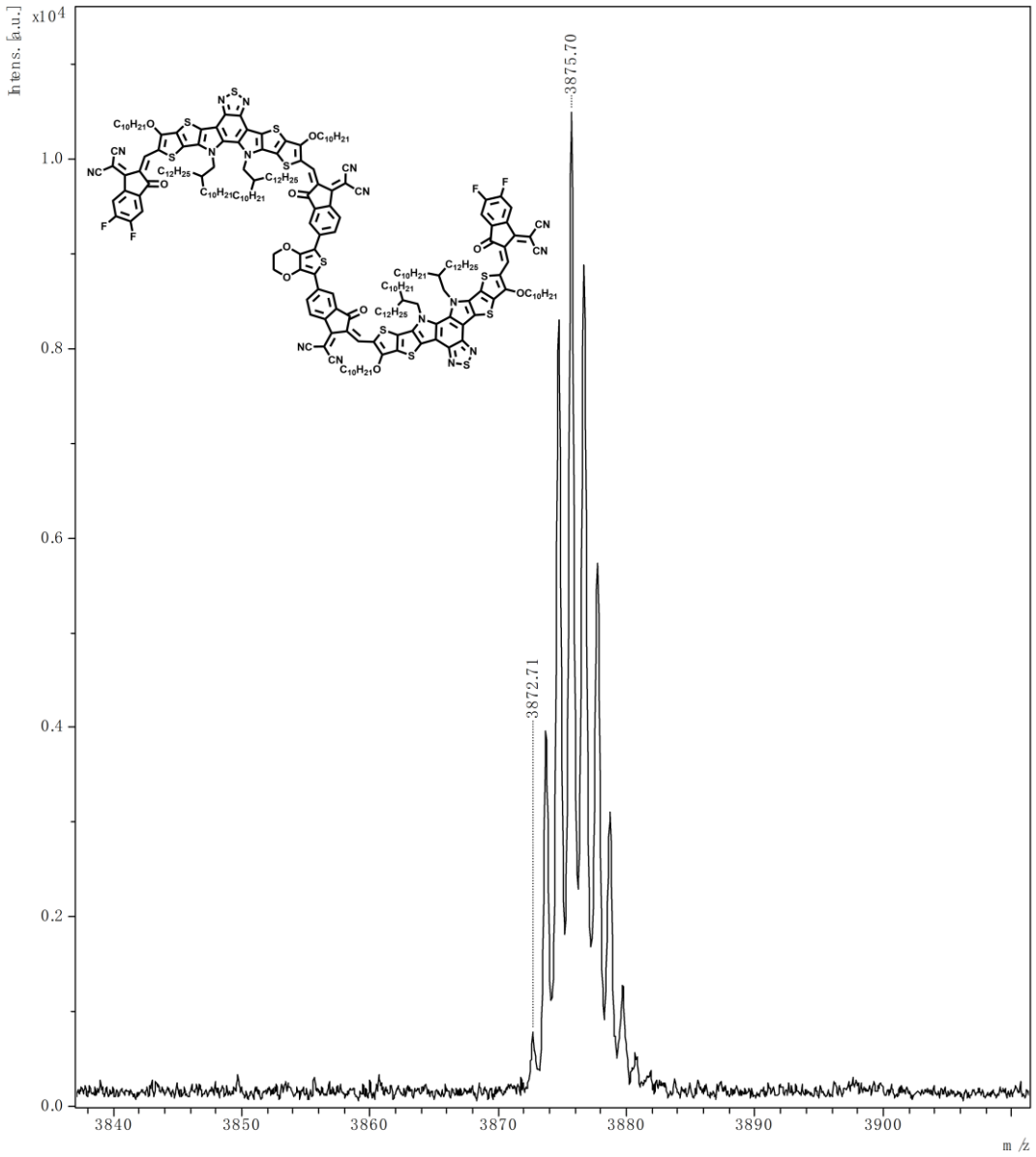

Figure S26. MS of DYO-1.

References

1. J. Yuan, Y. Zhang, L. Zhou, G. Zhang, H.-L. Yip, T.-K. Lau, X. Lu, C. Zhu, H. Peng, P. A. Johnson, M. Leclerc, Y. Cao, J. Ulanski, Y. Li and Y. Zou, *Joule*, 2019, **3**(4), 1140-1151.
2. M. J. Abraham, T. Murtola, R. Schulz, S. Páll, J. C. Smith, B. Hess and E. Lindahl, *SoftwareX*, 2015, **1-2**, 19-25.
3. B. Hess, H. Bekker, H. J. C. Berendsen and J. G. E. M. Fraaije, *J. Comput. Chem.*, 1997, **18**(12), 1463-1472.
4. M. Parrinello and A. Rahman, *J. Appl. Phys.*, 1981, **52**(12), 7182-7190.
5. S. Nosé, *J. Chem. Phys*, 1984, **81**(1), 511-519.
6. H. W., D. A. and S. K., *J. Mol. Graph.*, 1996, **14**(1), 33-38.